

**Rules for Biologically Inspired Adaptive Network Design**Atsushi Tero, *et al.**Science* **327**, 439 (2010);

DOI: 10.1126/science.1177894

*This copy is for your personal, non-commercial use only.*

**If you wish to distribute this article to others**, you can order high-quality copies for your colleagues, clients, or customers by [clicking here](#).

**Permission to republish or repurpose articles or portions of articles** can be obtained by following the guidelines [here](#).

**The following resources related to this article are available online at [www.sciencemag.org](http://www.sciencemag.org) (this information is current as of February 6, 2012):**

**Updated information and services**, including high-resolution figures, can be found in the online version of this article at:

<http://www.sciencemag.org/content/327/5964/439.full.html>

**Supporting Online Material** can be found at:

<http://www.sciencemag.org/content/suppl/2010/01/21/327.5964.439.DC1.html>

A list of selected additional articles on the Science Web sites **related to this article** can be found at:

<http://www.sciencemag.org/content/327/5964/439.full.html#related>

This article **cites 20 articles**, 2 of which can be accessed free:

<http://www.sciencemag.org/content/327/5964/439.full.html#ref-list-1>

This article has been **cited by 2** article(s) on the ISI Web of Science

This article has been **cited by 9** articles hosted by HighWire Press; see:

<http://www.sciencemag.org/content/327/5964/439.full.html#related-urls>

This article appears in the following **subject collections**:

Computers, Mathematics

[http://www.sciencemag.org/cgi/collection/comp\\_math](http://www.sciencemag.org/cgi/collection/comp_math)

16. J. A. Burns, P. L. Lamy, S. Soter, *Icarus* **40**, 1 (1979).
17. J. A. Burns, D. P. Hamilton, F. Mignard, S. Soter, in *Physics, Chemistry, and Dynamics of Interplanetary Dust*, ASP Conference Series 104, B. A. Gustafson, M. S. Hanner, Eds. (Astronomical Society of the Pacific, San Francisco, 1996), pp. 179–182.
18. B. J. Buratti, M. D. Hicks, K. A. Tryka, M. S. Sittig, R. L. Newburn, *Icarus* **155**, 375 (2002).
19. F. Tosi *et al.*, preprint available at <http://arxiv.org/abs/0902.3591> (2009).
20. Besides Iapetus, Hyperion, Titan, and outer-satellite impacts were suggested; see also (12).
21. Reference (18) mentions an increase of the dust flux by ~20%, whereas (35) finds as much as a factor of 3 for some cases.
22. D. J. Tholen, B. Zellner, *Icarus* **53**, 341 (1983).
23. The leading sides of the moons beyond Mimas and inside Titan should be substantially coated by E-ring particles (24, 36, 37), making them less useful for this argument.
24. B. J. Buratti, J. A. Mosher, T. V. Johnson, *Icarus* **87**, 339 (1990).
25. J. A. Burns *et al.*, *Science* **284**, 1146 (1999).
26. S. S. Sheppard, [www.dtm.ciw.edu/users/sheppard/satellites/satsatdata.html](http://www.dtm.ciw.edu/users/sheppard/satellites/satsatdata.html) (2009).
27. D. Nesvorný, J. L. A. Alvarez, L. Dones, H. F. Levison, *Astron. J.* **126**, 398 (2003).
28. D. Turrini, F. Marzari, H. Beust, *Mon. Not. R. Astron. Soc.* **391**, 1029 (2008).
29. A. J. Verbiscer, M. F. Skrutskie, D. P. Hamilton, *Nature* **461**, 1098 (2009).
30. This idea was developed in several papers (18, 38, 39), but under the assumption that dust from the outer saturnian moons formed Iapetus' albedo dichotomy.
31. T. V. Johnson *et al.*, *J. Geophys. Res. Solid Earth* **88**, 5789 (1983).
32. T. Denk, R. Jaumann, G. Neukum, in *Lisbon Euroconference Jupiter After Galileo and Cassini, Abstracts Book 17 to 21 June 2002*, Lisbon, Portugal, abstr. no. P-4.1.18, 2002, p. 118.
33. B. J. Buratti, J. A. Mosher, *Icarus* **90**, 1 (1991).
34. M. E. Davies, F. Y. Katayama, *Icarus* **59**, 199 (1984).
35. K. J. Zahnle, P. Schenk, H. Levison, L. Dones, *Icarus* **163**, 263 (2003).
36. K. D. Pang, C. C. Voge, J. W. Rhoads, J. M. Ajello, *J. Geophys. Res. Solid Earth* **89**, 9459 (1984).
37. D. P. Hamilton, J. A. Burns, *Science* **264**, 550 (1994).
38. P. C. Thomas, J. Veeverka, *Icarus* **64**, 414 (1985).
39. K. S. Jarvis, F. Vilas, S. M. Larson, M. J. Gaffey, *Icarus* **146**, 125 (2000).
40. G. Neukum, B. A. Ivanov, in *Hazards Due to Comets and Asteroids*, T. Gehrels, Ed. (Univ. of Arizona Press, Tucson, AZ, 1994), pp. 359–416.
41. T. Roatsch *et al.*, *Planet. Space Sci.* **57**, 83 (2009).
42. We acknowledge the individuals at CICLOPS (at the Space Science Institute in Boulder, CO) and JPL (Pasadena, CA), as well as the members and associates of the Imaging Team for the successful conduct of the ISS experiment onboard the Cassini spacecraft. This paper is dedicated to Steve Ostro, whose work helped considerably to explain the nature of Iapetus' dark terrain. This work has been funded by the German Aerospace Center (DLR) and NASA/JPL.

### Supporting Online Material

[www.sciencemag.org/cgi/content/full/science.1177088/DC1](http://www.sciencemag.org/cgi/content/full/science.1177088/DC1)  
SOM Text  
Figs. S1 to S8  
Tables S1 and S2  
References and Notes

1 June 2009; accepted 1 December 2009  
Published online 10 December 2009;  
10.1126/science.1177088  
Include this information when citing this paper.

## Rules for Biologically Inspired Adaptive Network Design

Atsushi Tero,<sup>1,2</sup> Seiji Takagi,<sup>1</sup> Tetsu Saigusa,<sup>3</sup> Kentaro Ito,<sup>1</sup> Dan P. Bebbler,<sup>4</sup> Mark D. Fricker,<sup>4</sup> Kenji Yumiki,<sup>5</sup> Ryo Kobayashi,<sup>5,6</sup> Toshiyuki Nakagaki<sup>1,6\*</sup>

Transport networks are ubiquitous in both social and biological systems. Robust network performance involves a complex trade-off involving cost, transport efficiency, and fault tolerance. Biological networks have been honed by many cycles of evolutionary selection pressure and are likely to yield reasonable solutions to such combinatorial optimization problems. Furthermore, they develop without centralized control and may represent a readily scalable solution for growing networks in general. We show that the slime mold *Physarum polycephalum* forms networks with comparable efficiency, fault tolerance, and cost to those of real-world infrastructure networks—in this case, the Tokyo rail system. The core mechanisms needed for adaptive network formation can be captured in a biologically inspired mathematical model that may be useful to guide network construction in other domains.

Transport networks are a critical part of the infrastructure needed to operate a modern industrial society and facilitate efficient movement of people, resources, energy, and information. Despite their importance, most networks have emerged without clear global design principles and are constrained by the priorities imposed at their initiation. Thus, the main motivation historically was to achieve high transport efficiency at reasonable cost, but with correspondingly less emphasis on making systems tolerant to interruption or failure. Introducing robustness inevitably requires additional redundant pathways that are not cost-effective in the short term. In recent years, the spectacular failure of key infrastructure

such as power grids (1, 2), financial systems (3, 4), airline baggage-handling systems (5), and railway networks (6), as well as the predicted vulnerability of systems such as information networks (7) or supply networks (8) to attack, have highlighted the need to develop networks with greater intrinsic resilience.

Some organisms grow in the form of an interconnected network as part of their normal foraging strategy to discover and exploit new resources (9–12). Such systems continuously adapt to their environment and must balance the cost of producing an efficient network with the consequences of even limited failure in a competitive world. Unlike anthropogenic infrastructure systems, these biological networks have been subjected to successive rounds of evolutionary selection and are likely to have reached a point at which cost, efficiency, and resilience are appropriately balanced. Drawing inspiration from biology has led to useful approaches to problem-solving such as neural networks, genetic algorithms, and efficient search routines developed from ant colony optimization algorithms (13). We exploited the slime mold *Physarum polycephalum* to develop a biologically inspired model for adaptive network development.

*Physarum* is a large, single-celled amoeboid organism that forages for patchily distributed food sources. The individual plasmodium initially explores with a relatively contiguous foraging margin to maximize the area searched. However, behind the margin, this is resolved into a tubular network linking the discovered food sources through direct connections, additional intermediate junctions (Steiner points) that reduce the overall length of the connecting network, and the formation of occasional cross-links that improve overall transport efficiency and resilience (11, 12). The growth of the plasmodium is influenced by the characteristics of the substrate (14) and can be constrained by physical barriers (15) or influenced by the light regime (16), facilitating experimental investigation of the rules underlying network formation. Thus, for example, *Physarum* can find the shortest path through a maze (15–17) or connect different arrays of food sources in an efficient manner with low total length (TL) yet short average minimum distance (MD) between pairs of food sources (FSs), with a high degree of fault tolerance (FT) to accidental disconnection (11, 18, 19). Capturing the essence of this system in simple rules might be useful in guiding the development of decentralized networks in other domains.

We observed *Physarum* connecting a template of 36 FSs that represented geographical locations of cities in the Tokyo area, and compared the result with the actual rail network in Japan. The *Physarum* plasmodium was allowed to grow from Tokyo and initially filled much of the available land space, but then concentrated on FSs by thinning out the network to leave a subset of larger, interconnecting tubes (Fig. 1). An alternative protocol, in which the plasmodium was allowed to extend fully in the available space and the FSs were then presented simultaneously, yielded similar results. To complete the network formation, we allowed any excess volume of plasmodium to

<sup>1</sup>Research Institute for Electronic Science, Hokkaido University, Sapporo 060-0812, Japan. <sup>2</sup>PRESTO, JST, 4-1-8 Honcho, Kawaguchi, Saitama, Japan. <sup>3</sup>Graduate School of Engineering, Hokkaido University, Sapporo 060-8628, Japan. <sup>4</sup>Department of Plant Sciences, University of Oxford, Oxford OX1 3RB, UK. <sup>5</sup>Department of Mathematical and Life Sciences, Hiroshima University, Higashi-Hiroshima 739-8526, Japan. <sup>6</sup>JST, CREST, 5 Sanbancho, Chiyoda-ku, Tokyo, 102-0075, Japan.

\*To whom correspondence should be addressed. E-mail: [nakagaki@es.hokudai.ac.jp](mailto:nakagaki@es.hokudai.ac.jp)

accumulate on a large FS outside the arena (LFS in Fig. 2A).

A range of network solutions were apparent in replicate experiments (compare Fig. 2A with Fig. 1F); nonetheless, the topology of many *Physarum* networks bore similarity to the real rail network (Fig. 2D). Some of the differences may relate to geographical features that constrain the rail network, such as mountainous terrain or lakes. These constraints were imposed on the *Physarum* network by varying the intensity of illumination, as the plasmodium avoids bright light (16). This yielded networks (Fig. 2, B and C) with greater visual congruence to the real rail network (Fig. 2D). Networks were also compared with the minimal spanning tree (MST, Fig. 2E), which is the shortest possible network connecting all the city positions, and various derivatives with increasing numbers of cross-links added (e.g., Fig. 2F), culminating in a fully connected Delaunay triangulation, which represents the maximally connected network linking all the cities.

The performance of each network was characterized by the cost (TL), transport efficiency (MD), and robustness (FT), normalized to the corresponding value for the MST to give  $TL_{MST}$ ,  $MD_{MST}$ , and  $FT_{MST}$ . The TL of the Tokyo rail network was greater than the MST by a factor of  $\sim 1.8$  (i.e.,  $TL_{MST} \approx 1.8$ ), whereas the average  $TL_{MST}$  for *Physarum* was  $1.75 \pm 0.30$  ( $n = 21$ ). Illuminated networks gave slightly better clustering around the value for the rail network (Fig. 3A). For comparison, the Delaunay triangulation was longer than the MST by a factor of  $\sim 4.6$ . Thus, the cost of the solutions found by *Physarum* closely matched that of the rail network, with about 30% of the maximum possible number of links in place. The transport performance of the two networks was also similar, with  $MD_{MST}$  of 0.85 and  $0.85 \pm 0.04$  for the rail network and the *Physarum* networks, respectively. However, the *Physarum* networks achieved this with marginally lower overall cost (Fig. 3A).

The converse was true for the fault tolerance ( $FT_{MST}$ ) in which the real rail network showed marginally better resilience, close to the lowest level needed to give maximum tolerance to a single random failure. Thus, only 4% of faults in the rail network would lead to isolation of any part, whereas  $14 \pm 4\%$  would disconnect the illuminated *Physarum* networks, and  $20 \pm 13\%$  would disconnect the unconstrained *Physarum* networks. In contrast, simply adding additional links to the MST to improve network performance resulted in networks with poor fault tolerance (Fig. 3B).

The trade-off between fault tolerance and cost was captured in a single benefit-cost measure, expressed as the ratio of  $FT/TL_{MST} = \alpha$ . In general, the *Physarum* networks and the rail network had a benefit/cost ratio of  $\sim 0.5$  for any given  $TL_{MST}$  (Fig. 3B). The relationship between different  $\alpha$  values and transport efficiency (Fig. 3C) highlighted the similarity in aggregate behavior of the *Physarum* network when considering all three performance measures ( $MD_{MST}$ ,  $TL_{MST}$ , and  $FT_{MST}$ ).

**Fig. 1.** Network formation in *Physarum polycephalum*. (A) At  $t = 0$ , a small plasmodium of *Physarum* was placed at the location of Tokyo in an experimental arena bounded by the Pacific coastline (white border) and supplemented with additional food sources at each of the major cities in the region (white dots). The horizontal width of each panel is 17 cm. (B to F) The plasmodium grew out from the initial food source with a contiguous margin and progressively colonized each of the food sources. Behind the growing margin, the spreading mycelium resolved into a network of tubes interconnecting the food sources.

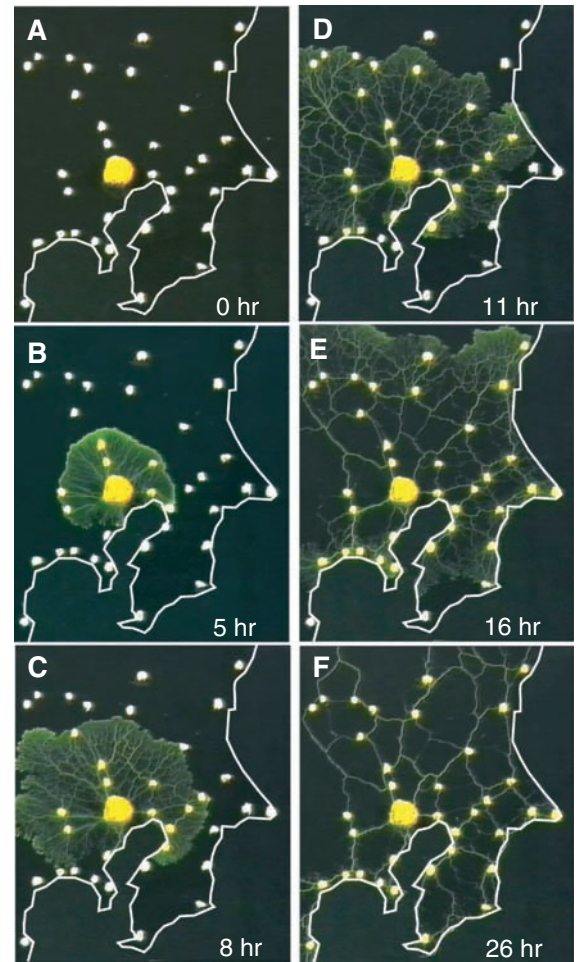


**Fig. 2.** Comparison of the *Physarum* networks with the Tokyo rail network. (A) In the absence of illumination, the *Physarum* network resulted from even exploration of the available space. (B) Geographical constraints were imposed on the developing *Physarum* network by means of an illumination mask to restrict growth to more shaded areas corresponding to low-altitude regions. The ocean and inland lakes were also given strong illumination to prevent growth. (C and D) The resulting network (C) was compared with the rail network in the Tokyo area (D). (E and F) The minimum spanning tree (MST) connecting the same set of city nodes (E) and a model network constructed by adding additional links to the MST (F).

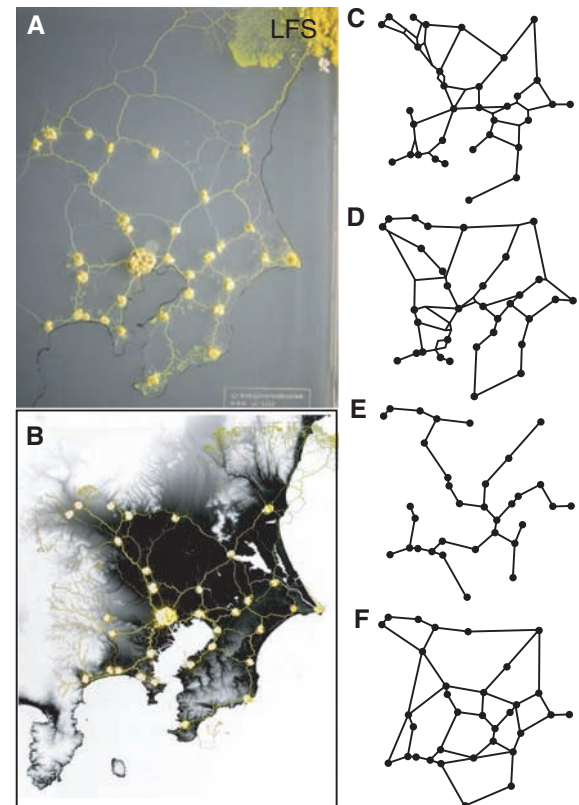
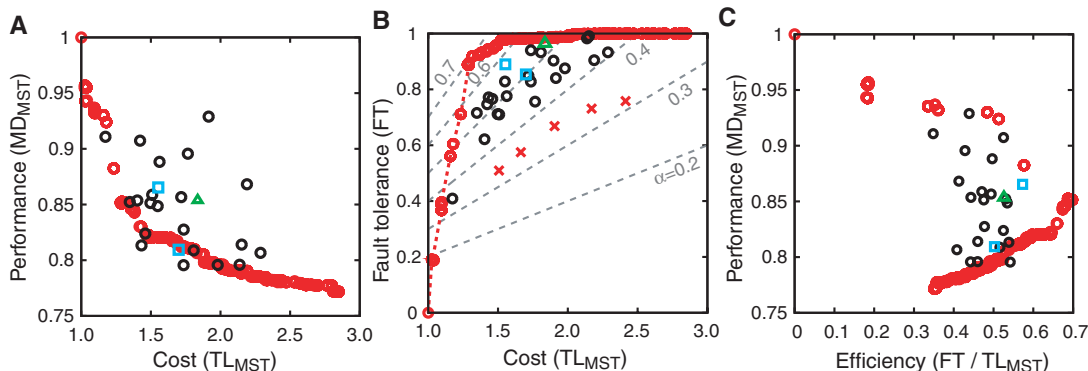
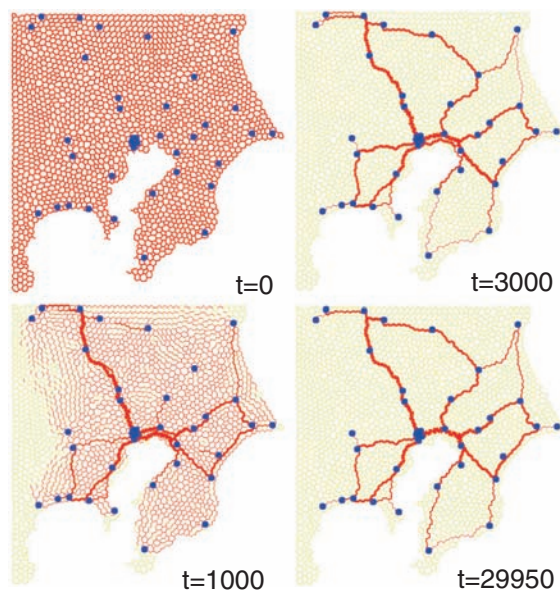


**Fig. 3.** Transport performance, resilience, and cost for *Physarum* networks, model simulations, and the real rail networks. (A) Transport performance of each network, measured as the minimum distance between all pairs of nodes, normalized to the MST ( $MD_{MST}$ ) and plotted against the total length of the network normalized by the MST ( $TL_{MST}$ ) as a measure of cost. Black circles and blue squares represent results obtained from *Physarum* in the absence or presence of illumination, respectively. The green triangle represents the actual rail network. Open red circles represent simulation results as  $I_0$  was varied from 0.20 to 7.19 at a fixed  $\gamma (= 1.80)$  and initial random fluctuations of  $D_{ij}$ . (B) Fault tolerance (FT), measured as the probability of disconnecting part of the network with failure of a single link. Crosses represent results for reference networks; other



symbols as in (A). Different values of the benefit/cost ratio,  $\alpha = FT/TL_{MST}$ , are shown as dashed lines. (C) Relationship between  $MD_{MST}$  and  $\alpha$ . Although the overall performance of the experiment and that of the real rail network are clustered together, the simulation model achieves better fault tolerance for the same transport efficiency.

**Fig. 4.** Network dynamics for the simulation model. In this typical time course for evolution of the simulation, time ( $t$ ) is shown in arbitrary units; cities are blue dots. Each city was modeled as a single FS, apart from Tokyo, which was an aggregate of seven FSs to match the importance of Tokyo as the center of the region. At the start ( $t = 0$ ), the available space was populated with a finely meshed network of thin tubes. Over time, many of these tubes died out, whilst a limited number of tubes became selectively thickened to yield a stable, self-organized solution.  $\gamma = 1.80$ ,  $I_0 = 2.00$ .



The rail network was embedded in the cluster of results for the *Physarum* networks with a marginally higher  $\alpha$  value for the same transport efficiency (Fig. 3C).

Overall, we conclude that the *Physarum* networks showed characteristics similar to those of the rail network in terms of cost, transport efficiency, and fault tolerance. However, the *Physarum* networks self-organized without centralized control or explicit global information by a process of selective reinforcement of preferred routes and simultaneous removal of redundant connections.

We developed a mathematical model for adaptive network construction to emulate this behavior, based on feedback loops between the thickness of each tube and internal protoplasmic flow (18–22) in which high rates of streaming stimulate an increase in tube diameter, whereas tubes tend to decline at low flow rates (23). The initial shape of a plasmodium is represented by a randomly meshed lattice with a relatively fine spacing, as shown in Fig. 4 ( $t = 0$ ). The edges represent plasmodial

tubes in which protoplasm flows, and nodes are junctions between tubes. Suppose that the pressures at nodes  $i$  and  $j$  are  $p_i$  and  $p_j$ , respectively, and that the two nodes are connected by a cylinder of length  $L_{ij}$  and radius  $r_{ij}$ . Assuming that flow is laminar and follows the Hagen-Poiseuille equation, the flux through the tube is

$$Q_{ij} = \frac{\pi r_{ij}^4 (p_i - p_j)}{8\eta L_{ij}} = \frac{D_{ij} (p_i - p_j)}{L_{ij}} \quad (1)$$

where  $\eta$  is the viscosity of the fluid, and  $D_{ij} = \pi r_{ij}^4 / 8\eta$  is a measure of the conductivity of the tube. As the length  $L_{ij}$  is a constant, the behavior of the network is described by the conductivities,  $D_{ij}$ , of the edges.

At each time step, a random FS (node 1) is selected to drive flow through the network, so the flux includes a source term  $\sum_j Q_{1j} = I_0$ . A second random FS is chosen as a sink (node 2) with a corresponding withdrawal of  $I_0$  such that  $\sum_j Q_{2j} = -I_0$ . As the amount of fluid must be conserved,

the inflow and outflow at each internal node must balance so that  $i (i \neq 1, 2)$ ,  $\sum_j Q_{ij} = 0$ . Thus, for a given set of conductivities and selected source and sink nodes, the flux through each of the network edges can be computed.

To accommodate the adaptive behavior of the plasmodium, the conductivity of each tube evolves according to  $dD_{ij}/dt = f(|Q_{ij}|) - D_{ij}$ . The first term on the right side describes the expansion of tubes in response to the flux. The second term represents the rate of tube constriction, so that in the absence of flow the tubes will gradually disappear. The functional form  $f(|Q|)$  is given by  $f(|Q|) = |Q|^\gamma / (1 + |Q|^\gamma)$ , which describes a sigmoidal response where  $\gamma$  is a parameter that controls the nonlinearity of feedback ( $\gamma > 0$ ). A typical simulation result with  $I_0 = 2$  and  $\gamma = 1.8$  (Fig. 4) gave a network with features similar to those of both the *Physarum* system and the rail network (Fig. 2, C and D, respectively).

In general, increasing  $I_0$  promoted the formation of alternative routes that improved performance by reducing  $MD_{MST}$  and made the network more fault-tolerant, but with increased cost (Fig. 3, A to C, and fig. S11). Low values of  $\gamma$  also gave a greater degree of cross-linking with an increased number of Steiner points (fig. S2, A and B). Conversely, decreasing  $I_0$  (fig. S1A) or increasing  $\gamma$  (fig. S2I) drove the system toward a low-cost MST (Fig. 2E), but with an inevitable decrease in resilience (Fig. 3B). The final network solution also depended slightly on the stochastic variation assigned to the starting values of  $D_{ij}$ . Judicious selection of specific parameter combinations ( $I_0 = 0.20$ ,  $\gamma = 1.15$ ) yielded networks with remarkably similar topology and metrics to the Tokyo rail network (fig. S2B). However, by increasing  $I_0$  to 2 and  $\gamma$  to 1.8, the simulation model also achieved a benefit/cost ratio ( $\alpha = FT/TL_{MST}$ ) that was better than those of the rail or *Physarum* networks, reaching a value of 0.7 with an almost identical transport efficiency of 0.85 (Fig. 3C). Conversely, the consequence of the increased  $TL_{MST}$  observed in the rail or *Physarum* networks would be to confer greater resilience to

multiple simultaneous failures at the expense of increased cost, rather than tolerance to a single disconnection that is evaluated by  $FT_{MST}$ .

Our biologically inspired mathematical model can capture the basic dynamics of network adaptability through iteration of local rules and produces solutions with properties comparable to or better than those of real-world infrastructure networks. Furthermore, the model has a number of tunable parameters that allow adjustment of the benefit/cost ratio to increase specific features, such as fault tolerance or transport efficiency, while keeping costs low. Such a model may provide a useful starting point to improve routing protocols and topology control for self-organized networks such as remote sensor arrays, mobile ad hoc networks, or wireless mesh networks (24).

#### References and Notes

1. R. Albert, I. Albert, G. Nakarado, *Phys. Rev. E* **69**, 025103R (2004).

2. R. V. Solé, M. Rosas-Casals, B. Corominas-Murtra, S. Valverde, *Phys. Rev. E* **77**, 026102 (2008).
3. R. M. May, S. Levin, G. Sugihara, *Nature* **451**, 893 (2008).
4. J. Kambhu, S. Weidman, N. Krishnan, *Econ. Policy Rev.* **13**, 1 (2007).
5. House of Commons Transport Committee, *The Opening of Heathrow Terminal 5 HC 543* (Stationery Office, London, 2008).
6. *Train Derailment at Hatfield* (Independent Investigation Board, Office of Rail Regulation, London, 2006).
7. R. Albert, H. Jeong, A.-L. Barabási, *Nature* **406**, 378 (2000).
8. R. Carvalho *et al.*, <http://arxiv.org/abs/0903.0195> (2009).
9. D. Bebbler, J. Hynes, P. Darrah, L. Boddy, M. Fricker, *Proc. R. Soc. London Ser. B* **274**, 2307 (2007).
10. J. Buhl *et al.*, *Behav. Ecol. Sociobiol.* **63**, 451 (2009).
11. T. Nakagaki, H. Yamada, M. Hara, *Biophys. Chem.* **107**, 1 (2004).
12. T. Nakagaki, R. Kobayashi, Y. Nishiura, T. Ueda, *Proc. R. Soc. London Ser. B* **271**, 2305 (2004).
13. A. Colomi *et al.*, *Int. Trans. Oper. Res.* **3**, 1 (1996).
14. A. Takamatsu, E. Takaba, G. Takizawa, *J. Theor. Biol.* **256**, 29 (2009).
15. T. Nakagaki, H. Yamada, Á. Tóth, *Nature* **407**, 470 (2000).
16. T. Nakagaki *et al.*, *Phys. Rev. Lett.* **99**, 068104 (2007).
17. T. Nakagaki, H. Yamada, Á. Tóth, *Biophys. Chem.* **92**, 47 (2001).

18. A. Tero, K. Yumiki, R. Kobayashi, T. Saigusa, T. Nakagaki, *Theory Biosci.* **127**, 89 (2008).
19. T. Nakagaki, R. Guy, *Soft Matter* **4**, 57 (2008).
20. T. Nakagaki, T. Saigusa, A. Tero, R. Kobayashi, in *Topological Aspects of Critical Systems and Networks: Proceedings of the International Symposium*, K. Yakubo *et al.*, Eds. (World Scientific, Singapore, 2007), pp. 94–100.
21. A. Tero, R. Kobayashi, T. Nakagaki, *J. Theor. Biol.* **244**, 553 (2007).
22. A. Tero, R. Kobayashi, T. Nakagaki, *Physica A* **363**, 115 (2006).
23. T. Nakagaki, H. Yamada, T. Ueda, *Biophys. Chem.* **84**, 195 (2000).
24. I. Akyildiz, X. Wang, W. Wang, *Comput. Netw.* **47**, 445 (2005).
25. Supported by MEXT KAKENHI grants 18650054 and 20300105, Human Frontier Science Program grant RGP51/2007, EU Framework 6 contract 12999 (NEST), and NERC grant A/S/882.

#### Supporting Online Material

[www.sciencemag.org/cgi/content/full/327/5964/439/DC1](http://www.sciencemag.org/cgi/content/full/327/5964/439/DC1)  
Figs. S1 and S2

17 June 2009; accepted 20 November 2009  
10.1126/science.1177894

# Measurement of Universal Thermodynamic Functions for a Unitary Fermi Gas

Munekazu Horikoshi,<sup>1\*</sup> Shuta Nakajima,<sup>2</sup> Masahito Ueda,<sup>1,2</sup> Takashi Mukaiyama<sup>1,3</sup>

Thermodynamic properties of matter generally depend on the details of interactions between its constituent parts. However, in a unitary Fermi gas where the scattering length diverges, thermodynamics is determined through universal functions that depend only on the particle density and temperature. By using only the general form of the equation of state and the equation of force balance, we measured the local internal energy of the trapped gas as a function of these parameters. Other universal functions, such as those corresponding to the Helmholtz free energy, chemical potential, and entropy, were calculated through general thermodynamic relations. The critical parameters were also determined at the superfluid transition temperature. These results apply to all strongly interacting fermionic systems, including neutron stars and nuclear matter.

Degenerate two-component Fermi systems with large scattering lengths are of great interest in diverse settings such as neutron stars (1–3), quark-gluon plasma (4), high critical temperature ( $T_c$ ) superconductors (5), and resonantly interacting cold Fermi gases near Feshbach resonances (6–18). Even though the temperature of these systems ranges widely from  $10^{-7}$  K for cold atoms to more than  $10^{12}$  K for quark-gluon plasma, they exhibit remarkably similar behavior at the unitarity limit. As the scattering length

diverges, the universal thermodynamics that describes these systems depends only on the particle density,  $n$ , and temperature,  $T$ . This assumption is referred to as the “universal hypothesis (UH)” (19, 20).

In the context of cold atoms, two fermionic alkali elements,  $^6\text{Li}$  and  $^{40}\text{K}$ , have been successfully used to explore the physics of the unitarity limit (6–18). This was possible because of the tunability of the fermion-fermion interaction and the stability of ultracold fermionic gases near Feshbach resonances (21, 22). Recently, a comparison of the entropy-energy relations extracted from experimental measurements on both  $^6\text{Li}$  and  $^{40}\text{K}$  provided evidence of universal thermodynamics at the unitarity limit (23). However, because a unitary Fermi gas is realized in a harmonic trap, the inhomogeneous atomic density distribution causes the thermodynamic quantities to be position-dependent.

Therefore, integration over the entire cloud provides only indirect information on the relationship between each individual thermodynamic quantity and the particle density. To determine the universal thermodynamic functions using such an inhomogeneous system, the thermodynamic

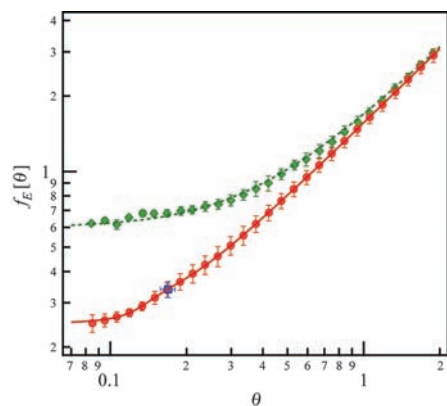


**Fig. 1.** Universal function of the internal energy. Universal functions of the internal energy ( $f_E[\theta] = E/N\epsilon_F$ ) plotted for an ideal Fermi gas (green diamonds) and for a unitary Fermi gas (red circles). The data are averaged over a suitable temperature range. The error bars show the data spread of one standard deviation originating mainly from statistical errors. The green dashed curve shows the theoretical universal function for the ideal Fermi gas, whereas the red solid curve shows the measured universal function for the unitary Fermi gas. The red solid curve is obtained by fitting the data represented by red circles so that it levels off at  $f_E[0] = 3(1 + \beta)/5 = 0.25$  at the low-temperature limit, where  $\beta$  is the universal parameter (15), and approaches the theoretical value obtained at the high-temperature limit (20). The blue square corresponds to the critical point.

<sup>1</sup>Japan Science and Technology Agency, Exploratory Research for Advanced Technology (ERATO), Macroscopic Quantum Control Project, 2-11-16 Yayoi, Bunkyo-ku, Tokyo 113-8656, Japan.

<sup>2</sup>Department of Physics, University of Tokyo, 7-3-1 Hongo, Bunkyo-ku, Tokyo 113-0033, Japan. <sup>3</sup>Center for Frontier Science and Engineering, University of Electro-Communications, 1-5-1 Chofugaoka, Chofu, Tokyo 182-8585, Japan.

\*To whom correspondence should be addressed. E-mail: hori@sogo.t.u-tokyo.ac.jp